13th International Symposium on Turbulence and Shear Flow Phenomena (TSFP13)
Montreal, Canada, June 25-28, 2024

MODIFICATION OF FLOW STRUCTURE AND ENERGY CASCADING PROCESS BY SMALL BUBBLES IN TURBULENT JETS

Hyunduk Seo
Eco-friendly Smart Ship Parts Technology
Innovation Center (EPIC)
Pusan National University
Busan 46241, Republic of Korea
hdseo0123@pusan.ac.kr

Kyung Chun Kim
School of Mechanical Engineering,
Eco-friendly Smart Ship Parts Technology
Innovation Center (EPIC)
Pusan National Univeristy
Busan 46241, Republic of Korea
kckim@pusan.ac.kr

ABSTRACT

In this study, we present the modification of the typical turbulent jet flow (Reynolds number = 3,174 at the source) by bubbles with a restricted condition (mean diameter ~ 1.7 mm, standard deviation ~ 0.18 mm, void fraction < 1% at the source). The tracer particles and bubbles are measured by using 4-D PTV, and the tracking data of the tracer particles are reconstructed into the regular grid space.

In the jet with added bubbles, small trivial vortical structures observed in the single-phase jet were not observed. But the extended turbulent energy cascading process beyond the wake frequency by the bubbles was observed. By loading a small number of bubbles in the turbulent jet, the turbulent intensity was suppressed and the energy of large-scale eddies was transported to the smaller scale eddies. It is notable that the wake frequency of the added bubbles is comparable to the intermediate scale of the jet turbulence (Taylor microscale) but, the extension ranged to much lower scales of them.

NTRODUCTION

One of the most interesting features of bubbles in turbulent bubbly flow is the bubble agitation due to their buoyancy and relative motions to the background liquid flows. The bubble agitation results in bubble-induced turbulence (BIT), so-called pseudo-turbulence, which can be differentiated from shear-induced turbulence (SIT) generated by the liquid flows. In this study, we conducted 4-D PTV of bubbly jets to characterize the effect of bubbles in a canonical turbulent jet flow. Bubbly jets (Re = 3,174 @ source) with low void fractions (0%, 0.66%, 1% @ source) and mono-dispersed bubbles (~1.72 mm in diameter) are issued from the bottom of a water tank and recorded by 4 high-speed cameras synchronized with illumination devices. The modifications of flow structure and energy cascading process are analyzed from the visualization of the three-dimensional vortical structures and comparing one-point velocity spectra.

EXPERIMENTAL SETUP

In this experiment, turbulent round jet is generated from a plain nozzle with diameter of 20 mm at the bottom of the water tank. For the cases of bubbly jet, bubbles are released from an array of six 32-gauge needles located at the end of the nozzle to generate small sized bubbles. Measurement of the turbulent jet is condcted by using four high-speed cameras (Vision research, VEO-410L & 710L, 1280 x 800 pixels with 0.116 um/pix) with low-pass filters (~ 550 um), orange color fluorescent tracer particles (Cospheric, 1.00 g/cc, 53-63 um), blue LED (Lavision, Flashlight-300), commercial white LED (80 W) arrays, and synchronizing system (Lavision, Davis 10.1 & PTU-X, 360 Hz). The illumination strategy for each phase is mostly similar to our previous experimental study (Kim et al. 2022). In this study, accurate measurement of each phase is achieved by operating blue LED and white LED arrays with a short delay (0.69 ms). The blue LED is used to illuminate the tracer particles, and the white LED is used to illuminate bubbles. It gives us the advantage of avoiding the overlap of signals from bubbles and particles. The schematic of the experimental setup is shown in figure 1. The signals from the particles and bubbles are tracked by using Shake-the-Box algorithms (Schanz et al. 2016). Before the tracking, geometric calibration is performed with a 2-plane calibration plate above the jet exit. The calibration accuracy is enhanced by using volume self-calibration and optical transfer function. It should be noted that the volume self-calibrations for the tracer particles and processed bubble image are separately performed since the reflection patterns on the bubble interfaces can be varied with the relative position of bubbles and cameras. The short delay of the bubble’s Lagrangian tracks is compensated by using spline functions, which is one of the bases of the Shake-the-box tracking algorithm. The particle tracks are reconstructed into a 2 mm regular Eulerian grid by using the VIC# method (Jeon et al., 2018) by optimizing flow field variables of the velocity-vorticity formulations of the incompressible and inviscid Navier-Stokes equation. The first and second order statistics are calculated from the chunked data recorded longer than 20 mins. One-point spectra are calculated from the time-resolved instances (Exp.330, 320). In Exp.300, 16 chunks of 800 time-resolved instances are used to calculate statistics and spectra. Specific experiment conditions are depicted in table 1.

Table 1. Experiment and recording conditions.

Case	Exp.330	Exp.320	Exp.300
Re_D		3,174	
Φ_0 (%)	1	0.66	0
Image acquisition	1. 100 chunks of 200 time-resolved images 2. 6,174 time-resolved		1&2. 16 chunks of 800 time-resolved images

	images		
Tracked particles	~12,000 particles/frame in 0.0135 m3		~8,000 particles/frame in 0.0135 m3
Tracked bubbles	~160/frame	~230/frame	-

VISUALIZATION OF VORTICAL STRUCTURES

In the present experiment, disturbances by the wakes of bubbles cannot be directly visualized but the comparison of large-scale flow motions between cases can be realized to diagnose the effect of bubbles in the jet. Figure 2 shows the identified vortical structure in each case. In the single-phase jet case (Exp.300), a series of ring-like vortices due to shear at the jet exit evolve with the jet stream. Since there is an erosion of the potential core attributed to the shear near the source, higher tortuosity has been induced. Part of the proceeded vortical structures ruptured and seems to have a typical tube-like (or "worms") shape. Eventually, those structures are broken down and form much smaller structures. Therefore, many typical coherent structures of a turbulent jet seem to be overlapped throughout the whole flow field (Nickels & Marusic, 2001). However, bubbly jet cases typically have thick coherent structures but rarely have structures as much as Exp.300 has. In Exp.330, there is intermittent stretching of the vortical structure near the source due to the higher initial buoyancy than Exp.320. In other words, the formation of the vortical structure near the jet source is dependent to the void fraction. However, the bubbles are eventually separated from the shear layer of the jet since each bubble has inherent upward momentum source, buoyancy. In downstream, each bubbly jet shows similar but different vortical structures: (1) both Exp.320 and Exp.330 still have relatively thick vortical structures (2) Exp.320 shows proceeded vortical structures from upstream but, Exp. 330 shows that the stretched vortical structures are recovered and populated around the jet.

LAGRANGIAN BUBBLE TRACKING

In bubbly flows, each individual bubble continuously produces wakes in the flow field. Those bubble wakes have been characterized by calculating collective wake instability frequency, f_{cwi}. The f_{cwi} was defined to represent that the large-scale bubble-induced eddies have a specific scale corresponding to the bubble size and the slip velocity (relative velocity) of the bubbles to the background flow (Riboux et al, 2013). The collective wake frequency f_{cwi} is defined as follows:

$$f_{cwi} = 0.14 u_{slip}/d_b \tag{1}$$

where u_{slip} is the slip velocity of bubble in the jet and d_b is the diameter of the bubble. In this study, the collective wake frequency can be calculated with a definition of the slip velocity as follows:

$$u_{slip} = \frac{1}{N_b}\sum_{i=1}^{N_b}(u_{b,i}(t,\mathbf{x}) - u_{w,i}(t,\mathbf{x})) \tag{2}$$

where N_b is the number of sampled bubbles, $u_{b,i}$ is the i-th bubble's velocity and $u_{w,i}$ is the water velocity corresponding to the location and time of the i-th bubble, $\boldsymbol{x}$ and t. In this study, we measured Lagrangian tracks of each bubble so that the direct characterization of the oscillation can be realized. We calculated Lagrangian energy spectra from more than 80 bubbles, which have a long continuous track over the measurement area (track length > 180), to see the bubble dynamics with a wide frequency range. Then, we can transform them into a frequency domain as shown in figure 3. The dashed lines show the collective wake frequency (f_{cwi} = 11.4 and 10.4 of Exp.330 and 320, respectively) of each bubbly jet case. The peak of the radial and azimuthal spectra shows a good agreement with the f_{cwi}. The result implies that the bubble oscillation and the collective wake frequency should be correlated. Meanwhile, we can also observe that the magnitude of the spectra has higher value at low frequency region, then collapsed to lower value at high frequency region. The magnitudes of all the spectra before f_{cwi} seem to be proportional to void fraction.

PROBABILITY DENSITY FUNCTION

One of direct tools to identify the existence of BIT is PDF (probability density function) of velocity fluctuations. It already has been proved by much research that the agitation from individual bubbles enhance intermittency then the PDF of axial velocity fluctuation will be skewed to positive due to the buoyancy of the bubbles. We also tried to examine the agitation by bubbles at specific radial locations since void fraction in the bubbly jet is not homogeneous. From now on, radial locations of the turbulent bubbly jet are classified according to the jet radius b where the water axial mean velocity profiles collapsed to 1/e of the centerline axial velocity: r = 0.1b is the jet core, r = b is the shear layer and r = 1.5b is the outer layer. (1) Many bubbles are populated and upward momentum is continuously supplied from upstream at the jet core. (2) At the shear layer, entrainment of the ambient fluid gets much dominant. Most of turbulent kinetic energies are produced inside the shear layer. (3) At the outer layer, direct perturbation from bubbles rarely exists. There will be both of radially propagated flow structures from the main jet stream.

Figures 4 and 5 show the PDF of radial and axial velocity fluctuation normalized by rms of each velocity components at z = 2D and z = 5D, respectively. Radial velocity fluctuations of the single-phase jet show Gaussian distribution and trivial splatting outmost the distribution. The Guassian distribution of the radial velocity fluctuation is not modified by adding the bubbles in the jet. However, the distribution of the axial velocity fluctuation shows differences between the single-phase jet and the bubbly jets. Axial velocity fluctuation of the single-phase jet shows negative skew (tails at left) inside the jet core but positive skew (taills at right) outside the jet core. By adding the bubbles inside the jet, well-known exponential tails at right inside the shear layer. But it is only observed in downstream (z = 5D). Furthermore, lowered left tails in the jet core is observed in bubbly jet cases. The observation represents that the enhanced upward intermittency can be dominated when the initial momentum of the jet became weaker than buoyancy.

IDENTIFICATION OF BIT FROM TURBULENT ENERGY SPECTRA

In this section, we would like to calculate relevant turbulent scales and diagnose the effect of the bubbles via turbulent spectra. To estimate the relevant flow scales, we adopted the Taylor's frozen turbulent hypothesis and the isotropy assumptions. First, viscous dissipation is estimated from the longitudinal second-order structure functions:

$$D_{ll} = C_2(\epsilon(r)r)^{2/3} \tag{3}$$

where C_2 = 2.1 is the Kolmogorov constant and $\varepsilon(r)$ is the viscous dissipation and r is the scale in length according to the Taylor frozen hypothesis at a specific location. An appropriate mean viscous dissipation $<\varepsilon>$ is estimated by figuring out a locally flat profile of the function:

$$\epsilon(r) = \frac{1}{r}\left[\frac{D_{ll}^2(r)}{C_2}\right]^{3/2} \tag{4}$$

Then we can obtain the Kolmogorov length scale $\eta = (\nu^3/<\varepsilon>)^{(1/4)}$, the Kolmogorov time scale $\tau_\eta = (\nu\ /<\varepsilon>)^{(1/2)}$, the Taylor microscale $\lambda = (30\ \nu\ u'_z{}^{2}/<\varepsilon>)^{0.5}$ and the Taylor Reynolds number $Re_\lambda = \lambda\ u'_{z,rms}/\nu$ and other turbulent scales. Figure 6 shows the normalized energy spectra of continuous phase at the shear layer (r = b). The normalized energy spectra correspond to typical energy spectra except for the extended cascading in high wavenumber range of bubbly jet cases. In the single-phase jet case, as the normalized wave number close to 1, the universal -5/3 slope is altered to much steep slope. Finally, very higher wave number region shows a little lifted tail due to noise. However, bubbly jet cases show extended -5/3 cascading process even the normalized wave number exceeds 1. It is noticeable that the magnitude of the spectra in the inertial subrange is little lower than the single-phase jet case. In bubbly flow, small number of bubbles sometimes cause "turbulent suppression" (reduction or attenuation of turbulent kinetic energy). Figure 7 shows energy spectra correspond to dimensional wavenumber. The bubbly jet cases have an extended cascading process beyond the Taylor microscale (black dashed line) of the single-phase jet and the bubble wake frequency (red dashed line). It is notable that the bubble wake frequency is between the Taylor microscale and the Kolmogorov length scale. The extended -5/3 cascading is different from the typical bubbly flows where the -3 subrange exists (Lance and Bataille, 1992; Alméras et al. 2017). It implies that the interaction between a small number of bubbles and jet structure can induce energy transfer to much smaller eddies but do not dominate the overall flow behavior since the flow is not buoyancy dominant flow like a bubble-driven plume flow. Furthermore, we can speculate that the turbulent suppression in this study seems to be realized from the combination of the scales of the small bubble wakes and comparable background flow scales (i,e, the scale of the bubbles is appropriate to carry the large-scale energy to the smaller scale eddies by means of wake interaction).

To identify the effect of the bubbles in terms of scales, premultiplied energy spectra normalized by the axial mean liquid velocity are calculated. Figure 8 shows the premultiplied spectra around the jet center (r = 0.1b). Both single-phase and bubbly jets cases show a peak of the bandwidth of each spectrum at kb = 1.5-3. However, the bubbly jets cases show a skewed distribution to a small wavenumber region and lifted tail at the high wavenumber region. Especially, the streamwise spectra and Reynolds shear-stress spectra of the bubbly jet has a plateau (Exp.320) or a minor peak (Exp.330) after the peak of the band. It may be attributed to the continuous production of the anisotropic bubble induced turbulence near the jet centerline at which most of the bubbles are populated. But it is confined to high wavenumber regions due to its scale. Figure 9 shows the premultiplied spectra at the shear layer (r = b). At the shear layer, there are still lifted tails of the energy spectra at high wavenumber regions depending on the void fraction. But no plateau is observed since the smaller portion of bubbles are populated around the shear layer than the jet core. It means that the extended cascading process is related to the collective wakes generated from individual bubbles. Also, overall turbulent intensity is suppressed due to the modification of the flow structures.

CONCLUSION

By adding bubbles in the turbulent jet, we observed the modification of flow structure and energy cascading process from the 3D flow visualization and one-point spectral analysis. In the visualization of the vortical structures, we can notice that the small vortical structures in the single-phase jet disappear in the jet with bubbles. In the one-point spectral analysis, we can notice that the -5/3 decaying extends beyond the scales of bubble wake and jet length scale. It seems that adding bubbles in the jet promotes further energy cascading process by means of interaction between the bubbles and jet structures. Some small-scale turbulence can be attributed to the direct dragging of the liquid by the bubbles but it is not dominant as much in the typical bubbly flows.

It is important to notice that the particle-laden flow rather shows the flow structures affect the dispersion of the particles, which are dragged or swept by flow structure (Longmire and Eaton, 1992). But we figured out that small fraction of bubbles shows significant modification in various ways. Furthermore, the size of the bubble is very important since the suppression of the turbulent kinetic energy and the extended cascading seem to have strong correlations with the bubble collective wake frequency.

REFERENCES

Alméras, E., Mathai, V., Lohse, D., & Sun, C. (2017). Experimental investigation of the turbulence induced by a bubble swarm rising within incident turbulence. *Journal of fluid mechanics*, *825*, 1091-1112.

Jeon, Y. J., Schneiders, J. F., Müller, M., Michaelis, D., & Wieneke, B. (2018). 4D flow field reconstruction from particle tracks by VIC+ with additional constraints and multigrid approximation. In *Proceedings 18th International Symposium on Flow Visualization*. ETH Zurich.

Kim, D., Schanz, D., Novara, M., Seo, H., Kim, Y., Schröder, A., & Kim, K. C. (2022). Experimental study of turbulent bubbly jet. Part 1. Simultaneous measurement of three-dimensional velocity fields of bubbles and water. *Journal of Fluid Mechanics*, *941*, A42.

Lance, M., & Bataille, J. (1991). Turbulence in the liquid phase of a uniform bubbly air–water flow. *Journal of fluid mechanics*, *222*, 95-118.

Longmire, E. K., & Eaton, J. K. (1992). Structure of a particle-laden round jet. *Journal of Fluid Mechanics*, *236*, 217-257.

Nickels, T. B., & Marusic, I.: On the different contributions of coherent structures to the spectra of a turbulent round jet and a turbulent boundary layer. *Journal of Fluid Mechanics*, 448, 367-385 (2001).

Riboux, G., Legendre, D., & Risso, F. (2013). A model of bubble-induced turbulence based on large-scale wake interactions. *Journal of Fluid Mechanics*, *719*, 362-387.

Schanz, D., Gesemann, S., & Schröder, A. (2016). Shake-The-Box: Lagrangian particle tracking at high particle image densities. *Experiments in fluids*, *57*, 1-27.

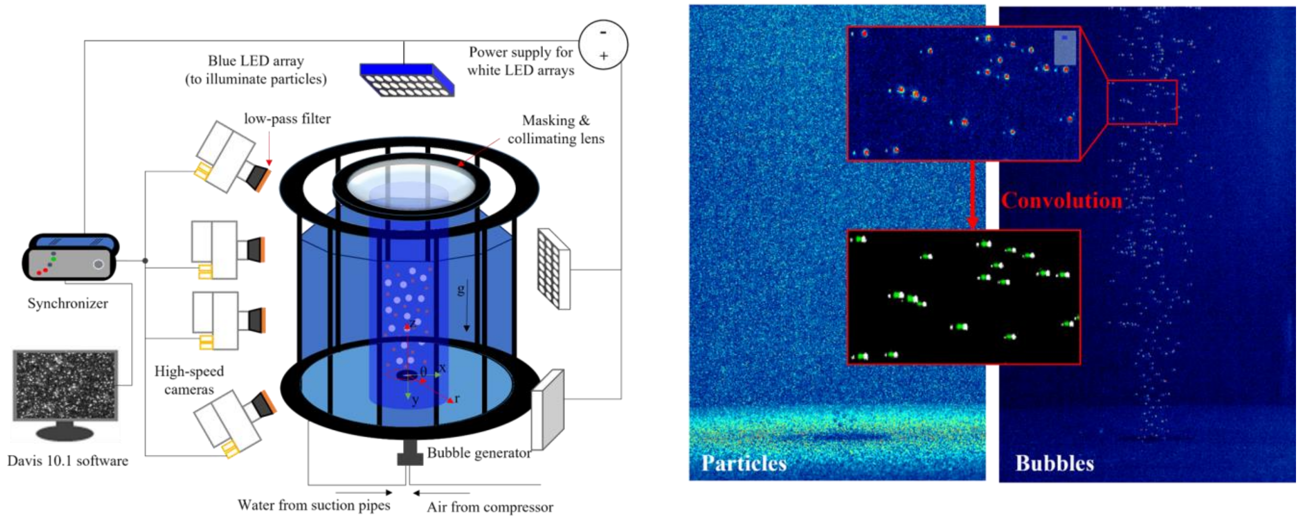

Figure 1. Experimental setup: (a) schematic of the experimental setup and (b) recorded particle and bubble images

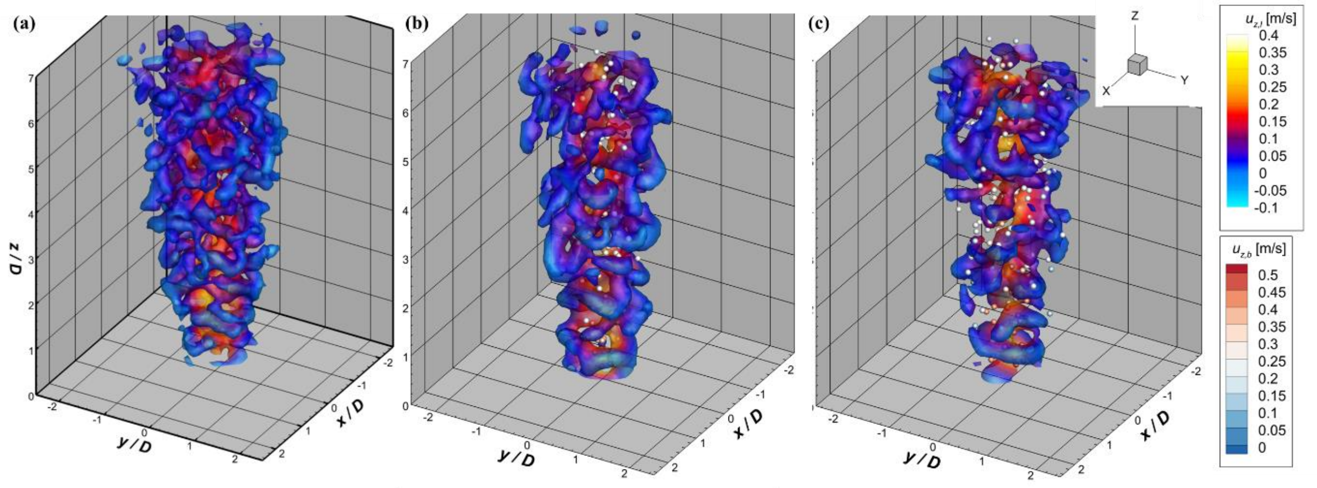

Figure 2 Identification of vortical structures in turbulent jets by Q-criterion (25 s-2). Iso-surfaces are color-coded by axial liquid velocity: (a) Exp.300; (b) Exp.320; (c) Exp.330. Tracked bubbles are color-coded by the axial bubble velocity.

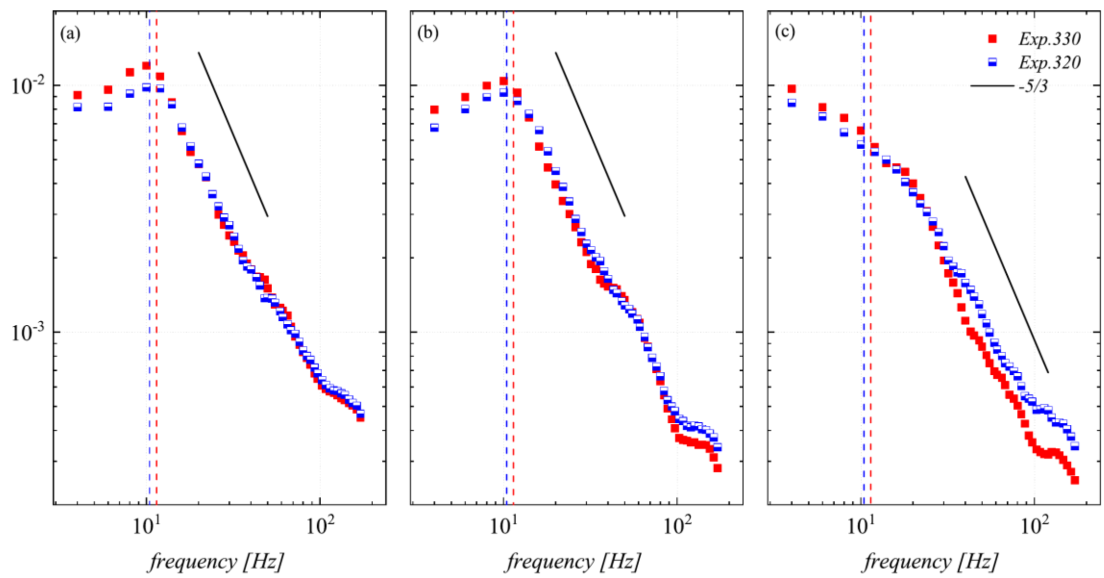

Figure 3 Averaged Lagrangian energy spectra from the sampled bubble tracks regarding to the (a) radial (b) azimuthal (c) axial velocity components.

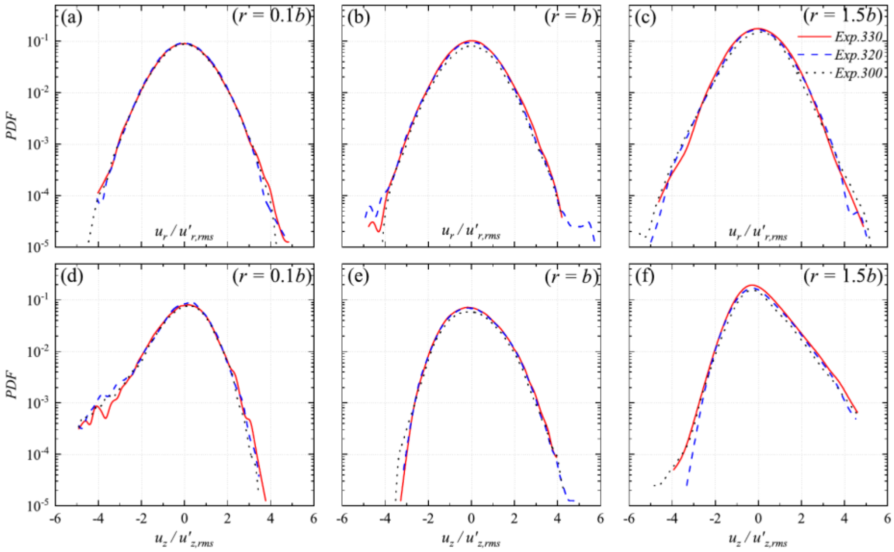

Figure 4 Probability density function of (a, b, c) radial liquid velocity fluctuations and (d, e, f) streamwise liquid velocity fluctuations at different radial locations in upstream (z = 2D). (a,d) jet core, (b,e) shear layer, (c,f) outer layer.

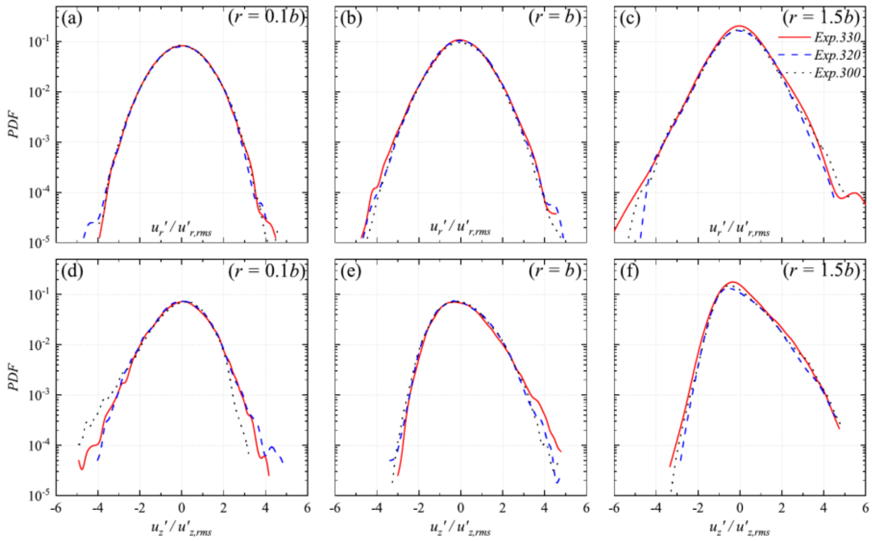

Figure 5 Probability density function of (a, b, c) radial liquid velocity fluctuations and (d, e, f) streamwise liquid velocity fluctuations at different radial locations in downstream (z = 5D). (a,d) jet core, (b,e) shear layer, (c,f) outer layer.

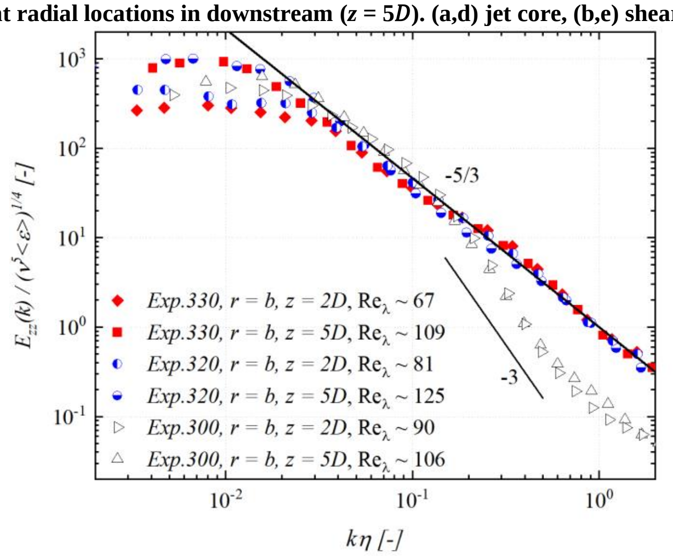

Figure 6 One dimensional longitudinal energy spectra $E_{11}(k)$ normalized by Kolmogorov scales. Kolmogorov's -5/3 power law is indicated by a solid line. Another solid line indicates -3 power for reference beyond the inertial subrange.

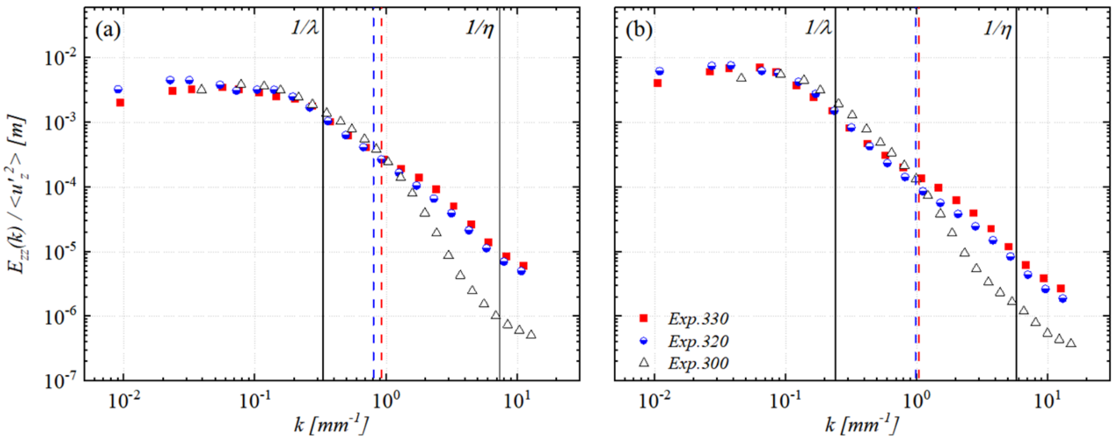

Figure 7. One dimensional energy spectra plotted against the wavenumber at shear layer (r = b): (a) z = 2D and (b) z = 5D. Blak solid lines refer to the Taylor microscale and the Kolmogorov length scale of Exp.300. Red and Blue dashed lines correspond to the f_{cwi} of Exp.330 and Exp.320, respectively.

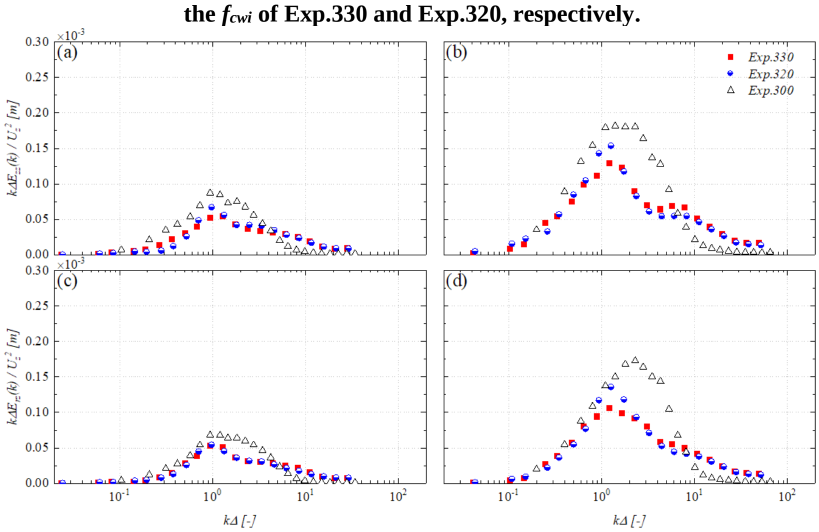

Figure 8. Premulitied energy spectra at jet core (Δ = 0.1b) extracted from (a, c) z = 2D and (b, d) z = 5D.

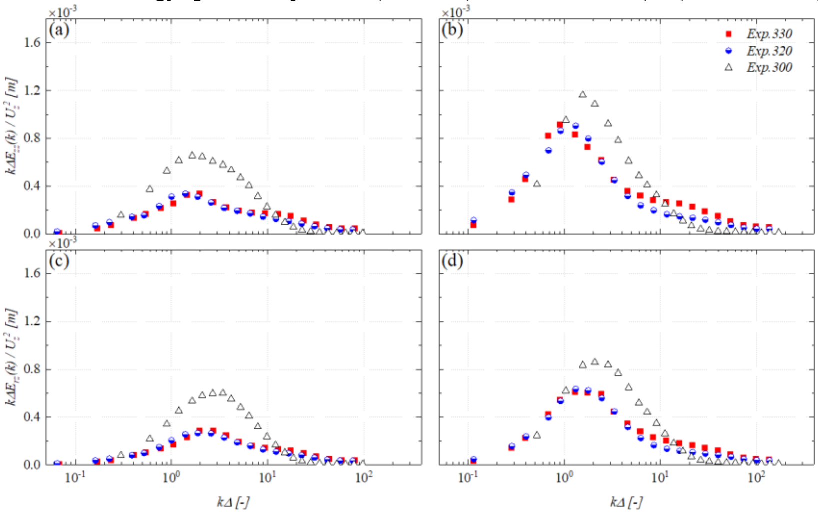

Figure 9. Premulitied energy spectra at shear layer (Δ = b) extracted from (a, c) z = 2D and (b, d) z = 5D.